HIGH EFFICIENCY Cu(In,Ga)Se$_2$-BASED SOLAR CELLS: PROCESSING OF NOVEL ABSORBER STRUCTURES

Miguel A. Contreras, John Tuttle, Andrew Gabor, Andrew Tennant, Kannan Ramanathan,
Sally Asher, Amy Franz, James Keane, L. Wang, John Scofield and, Rommel Noufi.
National Renewable Energy Laboratory, Golden, CO 80401

ABSTRACT

Our effort towards the attainment of high performance devices has yielded several devices with total-area conversion efficiencies above 16%, the highest measuring 16.8% under standard reporting conditions (ASTM E892-87, Global 1000 W/m^2). The first attempts to translate this development to larger areas resulted in an efficiency of 12.5% for a 16.8-cm^2 monolithically interconnected submodule test structure, and 15.3% for a 4.85-cm^2 single cell. Achievement of a 17.2% device efficiency fabricated for operation under concentration (22-sun) is also reported. All high efficiency devices reported here are made from graded bandgap absorbers. Bandgap grading is achieved by compositional Ga/(In+Ga) profiling as a function of depth. The fabrication schemes to achieve the graded absorbers, the window materials and contacting will be described.

INTRODUCTION

In this paper, we report on device optimizations that have led to important efficiency achievements. We present two different absorber fabrication approaches, which we believe represent promising and viable paths to large-area manufacturing of CuInSe$_2$ (CIS)-based modules. These processes are (1) coevaporation and (2) compound formation from Se containing precursors.

Regardless of the absorber fabrication process, all high efficiency Cu(In,Ga)Se$_2$ (CIGS) materials appear smooth and specular, with a morphology characterized by well-faceted and columnar grains. They always fall within a 0.86$\leq$Cu/(In+Ga)$\leq$0.96 compositional range—as determined by electron probe microanalysis (EPMA) and include compositional gradients in Ga/(In+Ga) as a function of depth. The graded Ga incorporation results in changes mostly in the conduction band (CB), hence, producing absorbers with graded bandgaps. X-ray diffraction (XRD) spectra show well-defined chalcopyrite structures without the presence of secondary phases (i.e., Cu$_2$Se, In$_2$Se$_3$). Capacitance-voltage (C-V) measurements also reveal graded doping profiles.

DEVICE PROCESSING

All devices reported in this contribution are fabricated with the layered structure shown schematically in Fig. 1. The base substrate of preference is soda-lime glass (SLG), but we have used other materials as well. Among them 7059 Corning glass, Al$_2$O$_3$, and metallic foils

such as Mo, Ni, and stainless steel. For terrestrial applications SLG has yielded the best results from a device performance point of view. In terms of lightweight flexible substrate—for potential space applications—Mo foils about 2.5x10^{-3} cm (0.001 in) thick have resulted in encouraging device performance results (efficiencies >10%). The most significant limitation for SLG substrates is its inability to withstand high processing temperatures (>500˚C). In some instances of our high efficiency absorber fabrication processes, samples are warped because of this thermally induced stress on the glass. We have partially addressed the problem by going to thicker SLG substrates (2-3 mm), but this situation could be more optimally solved by either lowering substrate temperature or finding other suitable and low-cost substrates.

Common to all 1-sun devices reported here, is the e-beam evaporated top-contact grid made of 500-Å Ni and 3-μm of Al. This top contact grid has about 4% shadowing loss. Details for the design of concentrator devices based on CIGS absorbers can be found in ref. [1]. A description of the other components in the CIS-based solar cell is presented below.

500-Å Ni + 3-μm Al grid

800-1300-Å MgF$_2$

0.35-0.5-μm n-ZnO
500-Å i-ZnO

500Å CdS

2-3.25-μm CIGS

1-2-μm Mo

2-3-mm Soda lime glass
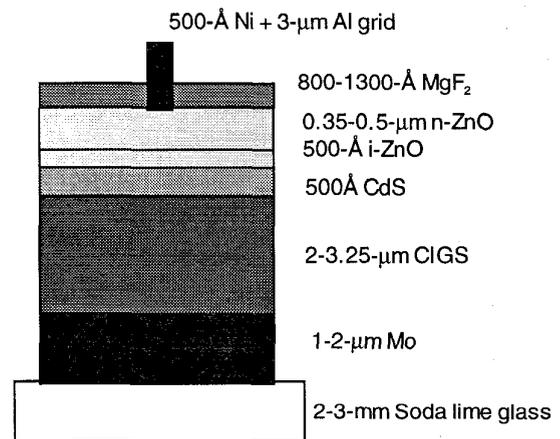
Fig. 1. Schematics of CIGS based solar cells

Mo Back Contact

The Mo back contact was fabricated by dc magnetron sputtering at two different Ar pressures

resulting in a 1μm bilayer. The first 0.1-μm is deposited at a pressure of 10 mTorr and exhibits good adhesion and a resistivity of about 60 μΩ-cm. The second layer (~0.9-μm) is deposited at 1 mTorr; it shows poor adhesion (to the SLG) and resistivity of 10 μΩ-cm. The resulting bilayer adheres very well to the SLG and retains the lower resistivity. Details of the deposition process and characteristics of the Mo bilayer can be found in ref. [2] of these proceedings.

ZnO and CdS window processing

The ~500-Å CdS layer deposited by a chemical bath deposition (CBD) technique has been described elsewhere[3].

Perhaps the most significant improvement on our window layers has come from an overall better quality ZnO. The ZnO is a bilayer structure composed of a thin (~500-Å) high resistivity i-ZnO film capped with a high conductivity n-ZnO layer (3500-5500 Å). The high resistivity layer is deposited by RF magnetron sputtering from an intrinsic ZnO target in a mixture of Ar and O_2 at a sputtering pressure of 10 mTorr with no intentional heating. The resistivity of the thin intrinsic layer is highly dependent on O_2 partial pressure during sputtering. The best results have been obtained with a highly dilute gas mixture with a concentration of less than 1% O_2. The doped ZnO layer is sputtered from a 2 wt% Al_2O_3-doped ZnO target with neither O_2 nor intentional heating. Typical sheet resistance for the 500-Å intrinsic layer, 3500-Å doped layer, and 4000-Å bilayer are 10^7, 25, and 15 Ω/sq., respectively. Characteristic transmission and reflection data of the doped layer ZnO window component are shown in Fig. 2.
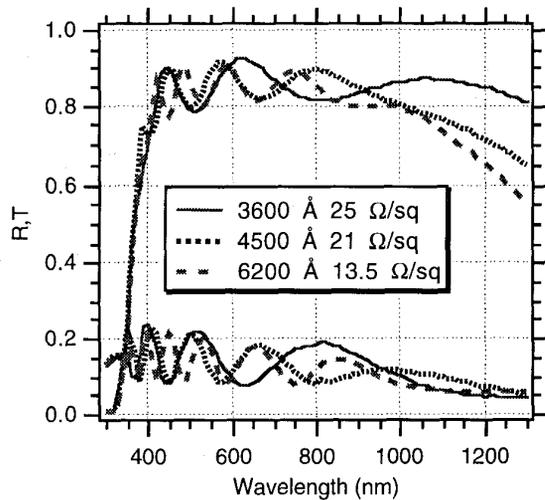
Fig. 2. Transmission and Reflection data obtained for doped ZnO of different thicknesses

Hall measurements performed on a 6300-Å thick n-ZnO sample, characterize the film with a 600-800 μΩ-cm resistivity, an electron density of 5.1-7.5 x10^{20} cm^{-3}, and a mobility of 14-15 cm^2/V-s. The measurement was done using a 2 Tesla magnetic field.

MgF$_2$ antireflection (AR) coating

The effect of the AR coating can be described as an effective optical coupling that allows more photons to reach the diode's junction with a net enhancement of current generation from the device. This coating is deposited by e-beam evaporation using optical-grade MgF$_2$ granules. Optimum thickness of this layer depends on the underlying ZnO properties and thickness. In our case—and for the ZnO quality we showed above—best results have been achieved with a MgF$_2$ thickness of 800-1200 Å. The gain in short circuit current is usually 4%-8% with the corresponding enhancement in conversion efficiency.

ABSORBER FABRICATION

Use of evaporation from elemental sources has proved to be a very flexible and powerful technique to explore different reaction pathways to compound formation and to fabricate specific graded band-gap absorbers in the CIGS system. Our focus on absorber fabrication for the past year covers two main approaches: (i) coevaporation, and (ii) CIGS formation from Se-containing precursors.
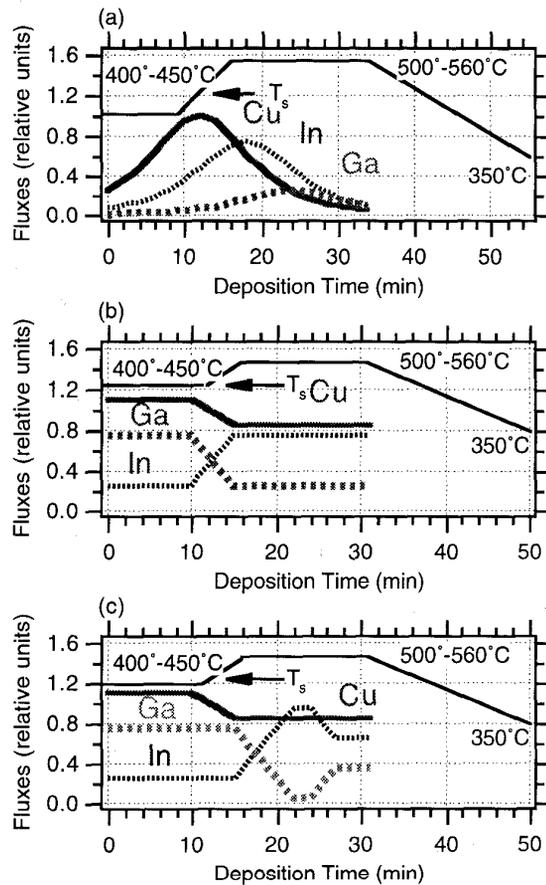
Figure 3. Deposition schemes for: (a) in-line emulation, (b) profiles for a normal grading, and (c) double grading

Coevaporation

This type of processing, enhanced by a computer interface for evaporant species deposition control, has allowed us to emulate potential large-scale in-line evaporation processes [4,5]. Furthermore, with the precise control of the metal fluxes during deposition—via preprogrammed profiles—we have been able to fabricate absorber materials that intentionally incorporate a compositional gradient in Ga/(Ga+In) as a function of depth.

Fig. 3 shows three coevaporation schemes with which we have experimented: (a) emulation of in-line coevaporation, (b) profiles for an absorber with normal band-gap grading, and (c) profiles for an absorber with double band-gap grading. The terms "normal" and "double grading" have been borrowed from amorphous Si (a-Si) technology where these type of graded band-gap structures have been previously implemented [6]. Common to all three coevaporation processes is a Se vapor selenization step done while cooling from the high substrate temperature (500°-560°C) to 350°C in 20 min.

The in-line coevaporation approach emulates a continuous evaporation process in which a substrate travels at a constant speed over the sources that evaporate at a constant rate. CIGS-based graded band-gap materials have been shown to enhance some device parameters [7] as well as improve adhesion [8] to the Mo/SLG substrate. Graded structures with normal- and double-graded profiles are discussed later in this paper in terms of a simple but highly idealized one-dimensional solar cell model.

CIGS formation from Se-containing precursors

First attempts to compound formation by this kind of reaction pathway were done in two stages. The first stage, done at a low substrate temperature (250°C<Ts<300°C), forms an $(In_{1-x}Ga_x)_2Se_3(s)$ precursor layer (0<x<0.30). This Se-containing precursor is then subjected —in a second stage—to a Cu and Se flux, along with a higher substrate temperature (500°C<Ts<560°C) to form the CIGS compound. We note that, in both stages the Se flux was three times that of the metals. The compound formation can be represented by the following generic equations:

$(In,Ga)(l)+Se(g) ---> (In_{1-x}Ga_x)_2Se_3(s)$
$(In_{1-x}Ga_x)_2Se_3(s) + Cu(s) + Se(g)-->Cu(In,Ga)Se_2(s)$
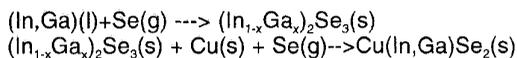
XRD data for a film obtained from the first-stage processing described above clearly reveals the crystallographic structure of an $(In_{1-x}Ga_x)_2Se_3(s)$ phase (see Fig. 4). Morphology and film evolution during Cu incorporation have been described in ref. [9,10].

The driving idea in this type of processing is to simplify manufacturing. It is conceivable to deposit the $(In_{1-x}Ga_x)_2Se_3$ precursor layer and the subsequent Cu-Se at low substrate temperatures by well-developed sputtering techniques, for example. A high-substrate temperature selenization step (via Se vapor or H_2Se) will then be required for compound formation and recrystallization.

This two-stage approach proved useful in fabricating thin films with near stoichiometric composition but with a rather small grain morphology and rough surfaces. A rough surface morphology may affect the device performance adversely because it can lead to poor metallurgical contact at the window/absorber interface. Furthermore, the added area at the junction will increase the forward current. Best devices fabricated by this two stage approach resulted in efficiencies <10%.
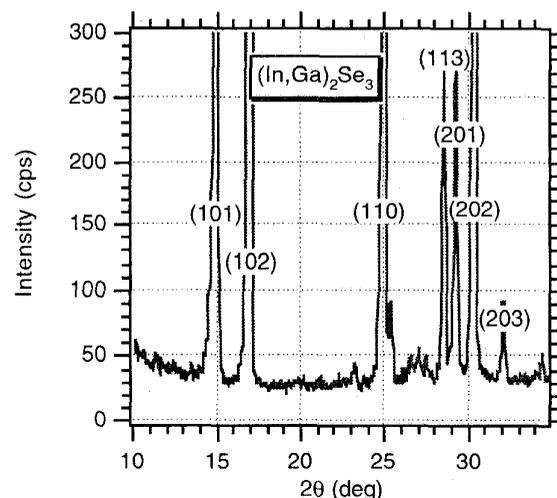
Fig. 4. XRD spectra of the $(In_{1-x}Ga_x)_2Se_3$ precursor film.

To improve bulk and surface morphology, we designed a 3-stage approach [11,12] in which a Cu-rich regime is reached at some point during Cu-Se deposition (second stage). We have previously reported on a growth model for CIS where we invoked the existence of a Cu_xSe liquid-phase as a fluxing agent that aids in grain growth [13]. This liquid-phase-assisted film growth yields a large and columnar grain morphology (see ref. [5,9,14]). Based on this premise, we decided to incorporate about 80%-90% of the In and Ga during the first stage, and the remaining 20%-10% after the completion of the second stage (see Fig. 5). With this scheme, the Cu-rich film at the end of the second stage consists of large-grain mixed phase of $Cu(In,Ga)Se_2$ and $Cu_{2-x}Se$.
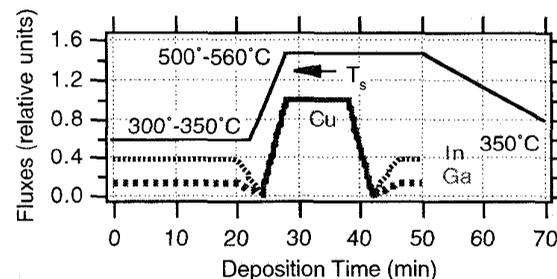
Fig. 5. Flux profiles for 3-stage processing

Adding the final 20%-10% of In and Ga at the end (third stage) is expected to aid in the formation of a smooth surface and to facilitate the formation of a Cu-poor

defect chalcopyrite that has previously been shown to exist at the surface of CIS films [15]. The process also includes a final Se vapor treatment while cooling from 560°C to 350°C in 20 min.

We note that the 3-stage processing results in absorbers with a graded bandgap structure with double profiling in Ga (see next section). The incorporation of graded Ga and In as a function of depth has been reported elsewhere (see ref. [11,12]).

Fig. 6 shows the representative morphology for a high-efficiency absorber made by the 3-stage processing approach. There are two aspects to this morphology: (1) columnar grains that facilitate current transport across the thickness of the absorber, and (2) a rather densely packed microstructure free of pinholes and microcracks.
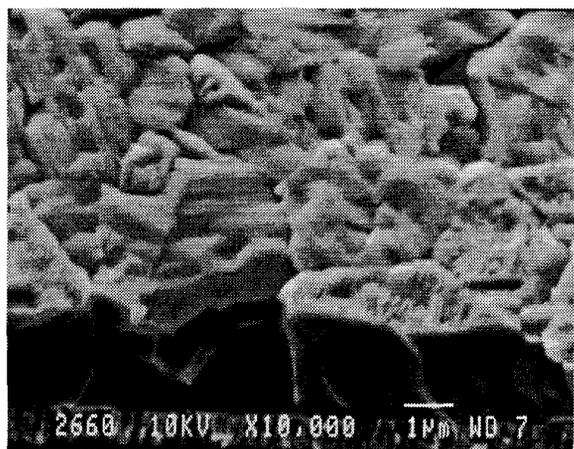
Fig. 6. SEM of film grown by 3-stage processing

XRD analysis (see Fig. 7) of absorbers grown by this 3-stage processing reveals a well-defined chalcopyrite structure with a strong (112) orientation and free of secondary phases (e.g., In_2Se_3, $Cu_{2-x}Se$)
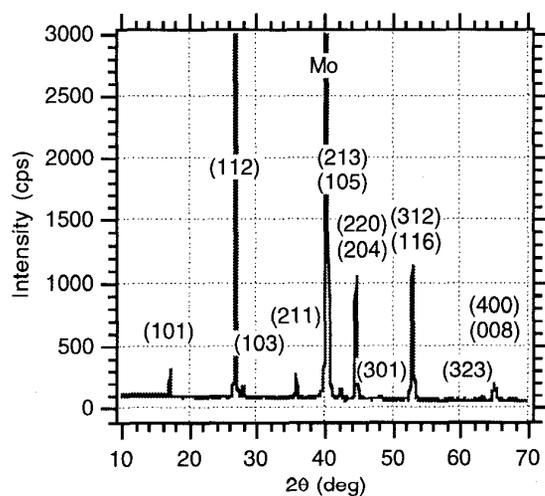
Fig. 7. XRD spectra of CIGS absorber

GRADED BAND-GAP STRUCTURES

Exchange of In atoms by Ga atoms in a base CIS matrix results in band-gap enhancement by raising mostly the conduction band (CB) edge [16]. In some cases, we have intentionally profiled Ga through the bulk of the film and, in others, compositional gradients were a result of the different diffusion mechanisms of In and Ga [10] during film growth (3-stage process). Graded Ga incorporation as a function of depth has implications on the shape of energy bands (conduction and valence) within the absorber structure. There are two types of band-gap grading we have focused upon. These are (a) normal profiling and (b) double profiling. These graded band-gap structures have been previously modeled and applied to a-Si:Ge alloys (see ref. [6]), with significantly enhanced device performance as compared to single band-gap absorbers. In the following paragraphs, we discuss both structures and their influence on device performance.

Normal grading structure

An absorber with normal profiling (nomenclature after ref. 6) is one where the band-gap is increased from front to back (see Fig. 8). The natural tendency of an electron excited to the CB will be to "roll down" the potential edge. The force exerted on such an electron comes from the additional quasi-electric field (due to the potential difference in the CB), and it can be seen intuitively from Fig. 8. The force acting on electrons in the CB (in p-type absorbers) is foreseen to "push" the electrons toward the space charge region and to reduce recombination at the back contact. Hence, the probability of these minority carriers contributing to current generation can be enhanced.
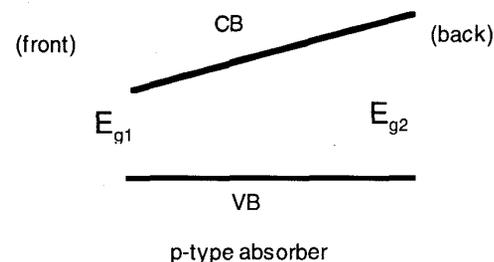
Fig. 8. One-dimensional band diagram of absorber incorporating normal profiling

To utilize the normal profiling concept in CIGS materials, we engineer a higher Ga content toward the back of the CIGS absorber (as shown in Fig. 3b). Because of the arguments presented above, this will result in an increase in the CB edge and the attainment of an effective force field repelling minority carriers from the back contact.

We have fabricated several absorbers that incorporate a higher Ga content toward the back of the device. Evidence of the graded Ga concentration has been verified using XRD and depth profiling techniques such as Auger Electron Spectroscopy (AES) (see Fig. 9) and Secondary Ion Mass Spectrometry (SIMS). Fig. 9a

shows the XRD spectra of the (112) peak for one of the normal profiling absorbers (sample S423). The XRD data reveal clearly the existence of at least two different CIGS compositions. Figure 9b is the Auger depth profile of the same absorber. Included in the figure are the EPMA results for accelerating voltages of 10 and 20 kV. The depth profile clearly shows a significant variation in Ga and In through the depth of the film. The lower Ga content found at the surface provides the lower band-gap composition. The higher Ga content found towards the back gives the wider band-gap composition. The compositional depth profile is complimentary to XRD data and serves as a qualitative verification of the normal profiling structure.

(b)

Depth (µm)
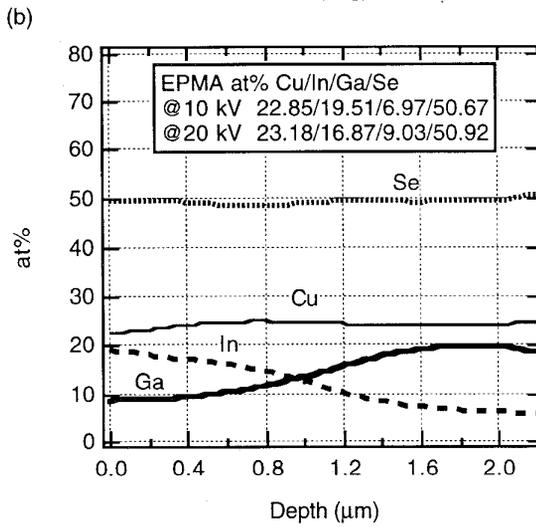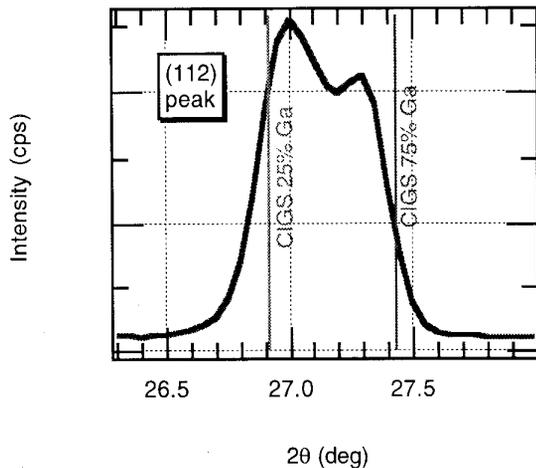
Fig. 9. (a) (112) peak XRD spectra of normal profiling absorber (sample S423), and (b) Auger depth profile for the same sample

Absorber with Double Profiling

The double profiling structure incorporates normal profiling plus an inverse profiling (reverse of a

normal profiling) in the region adjacent to the surface of the film (see Fig. 10). The first absorbers incorporating this type of structure were fabricated by the coevaporation process shown in Fig. 3(c), but also have been attained by the 3-stage scheme shown in Fig. 5. This double profiling structure has been theoretically modeled in a-Si devices [in Ref. 6]. The authors conclude that a double-profiled structure with a front graded a-Si layer extended for about 10%-20% of the total device thickness should give improved performance over simple unidirectional profiling.

A particular case of this double profiling is a notch structure. The latter can be thought of as a low band-gap material sandwiched between two wider band-gap materials. A theoretical analysis and numerical computer simulations of this and other graded structures based on CIGS has been reported by Dhingra *et al.* [17]. Among all the different simulations carried out by these authors, the notch structure yields the highest projected device performance.
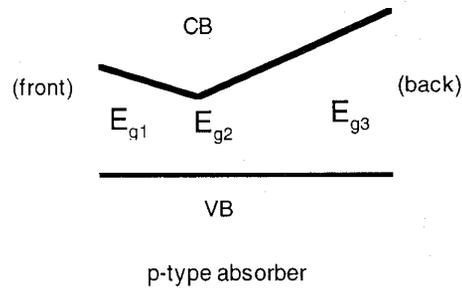
Figure 10. One-dimensional band diagram of absorber incorporating double profiling

Referring to Fig. 10, we anticipate the double profiling structure to absorb photons with energies higher than E_{g1}; furthermore, due to a decreasing energy gap as a function of depth, we can expect some of the photons with energies as low as E_{g2} to be absorbed ($E_{g1}>E_{g2}$). Hence, the structure has the potential for optimized photon absorption in a specific photon energy range.

The two energy gaps at the front of the double profiling structure (E_{g1} and E_{g2} in Fig. 10), could be engineered to match certain bands of the terrestrial solar spectrum (AM1.5) in order to capture more efficiently from the blue and red spectral regions. The improved quantum efficiency in such a device will translate into enhanced current generation (increase in J_{sc}). An additional enhancement of current generation could also come from the force field effect on electrons created by the increasing CB edge found towards the back (similar to the normal profiling structure discussed above).

Fig. 11 shows the SIMS depth profile for an absorber incorporating double profiling (sample C266) fabricated using the 3-stage process. The SIMS profile is calibrated with a set of standards with known compositions (as determined by EPMA). This method results in quantitative accuracy of ±1 at% for Ga and In, and ±3 at% for Cu and Se. The analysis clearly reveals the qualitative aspect of the double profiling structure. Atomic composition (at%) of the same film (C266) as obtained from EPMA are:

72

Cu/In/Ga/Se=23.25/18.83/7.73/50.20 at 10 kV and 22.82/19.67/6.96/50.56 at 20 kV.

The model adopted in ref. [17] points out an optimum notch position as close as possible to the front surface. The depth profile in Fig. 11 meets this condition to some degree. There are, however, questions regarding the optimum width and depth of the notch, variables that we continue to investigate along with abrupt transitions between different compositions.

DEVICE PERFORMANCE

Table 1 is a summary of I-V measurements for representative small-area devices. All I-V parameters reported in the table are for total-area measurements under standard reporting conditions of 1000 Wm^{-2} irradiance and a cell temperature of 25°C (ASTM E892). The table includes the "effective" bandgap value as obtained from cut-off extrapolation of the quantum efficiency measurements. In the table, we also include results on a 22-sun concentrator device. Table 2 is a summary of I-V results for larger area devices.
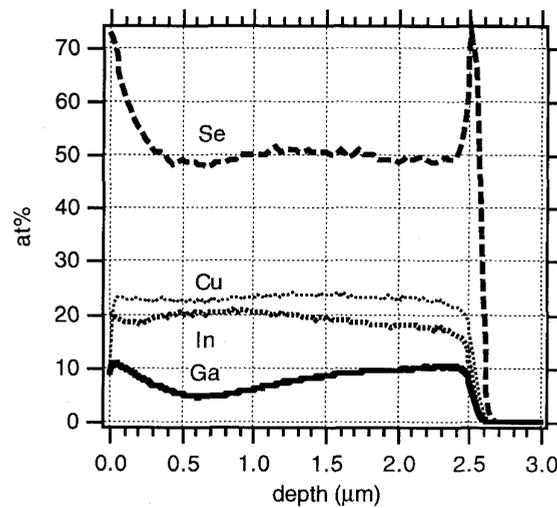
Fig. 11. SIMS depth profile of absorber incorporating double profiling (sample C266)

sample	type of grading	area (cm^2)	V_{oc} (mV)	J_{sc} (mA/cm^2)	FF (%)	Total Area Efficiency (%)	E_g (eV)
M1201	CuInSe$_2$ (no Ga)	0.395	484	36.29	75.10	13.2	0.95
S456	normal on Mo foil	0.444	496	32.93	62.70	10.2	1.07
S319	normal	0.251	**687**	23.73	74.78	12.2	1.17
S423	normal	0.422	664	29.24	78.04	15.1	1.10
C253	double	0.432	611	**34.13**	76.00	15.8	1.03
C257	double	0.458	623	32.82	75.36	15.4	1.07
C266	double	0.418	660	31.53	**78.73**	16.4	1.08
C362	double	0.437	652	33.18	77.44	**16.8**	1.09
C364	22-sun concent.	0.074	0.767	49.68	75.2	17.2	-
C371-14	double	1.025	678	31.96	75.80	16.4	1.11

Table 1. I-V parameters obtained under standard reporting conditions of 25°C and irradiance of 1000 W/m^2 (ASTM E892). Concentrator cell is a grided device with 15% shadowing.

comments	area (cm^2)	V_{oc} (V)	I_{sc} (mA)	FF (%)	Efficiency (%)
submod. 6 cells	16.8	3.43	92.1	66.3	12.5
single cell	6.64	0.644	198.5	72.21	13.9
single cell	4.85	0.657	150.7	74.75	15.3

Table 2. I-V parameters for larger area devices. Submodule structures incorporate a monolithic interconnection between cells.

From Table 1, we note that devices incorporating a double profiling absorber preserve the high V_{oc} values attained in the normal profiling devices, moreover, they yield higher short-circuit currents for comparable effective band-gaps. This situation can be explained from the enhanced spectral response of the double profiling

structures. Fig. 12 shows the normalized quantum efficiency (QE) of selected normal and double profiling devices. The figure reveals that normal profiling devices do not collect efficiently in the long wavelengths. The double profiling devices on the other hand, not only have an improved response in the long wavelengths but in the short wavelengths as well. However, we like to emphasize that we have not explored extensively other normal profiling schemes which might improve the red response. The short wavelength cutoff is common to all devices and is only limited by the transmission properties of the interface window material (CdS).

To calculate carrier concentration from capacitance data (in polycrystalline materials) we have followed the approach described in ref. [18]. Carrier concentrations in the CIGS graded structures are determined mostly by the film compositions resulting from the growth conditions described above.
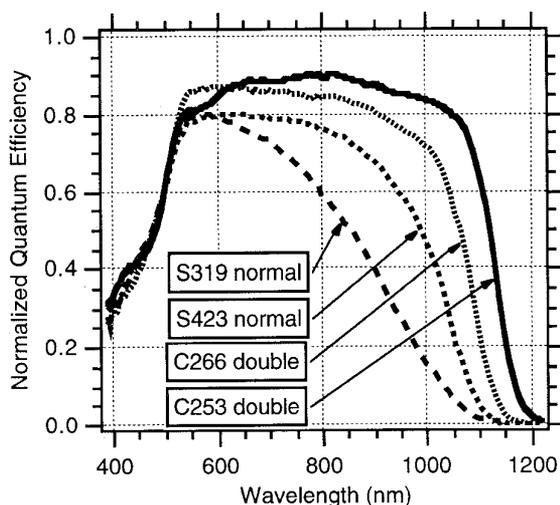
Fig. 12. Normalized QE for selected devices incorporating absorbers with normal and double profiling

Capacitance measurements of all graded band-gap devices reveal a graded carrier concentration profile. Fig. 13 shows the carrier concentration as a function of distance from the space charge edge for both graded structures (normal and double profiling).

FINAL REMARKS

The results presented above are very encouraging. For absorber band gaps used in this study, device parameters exist for greater than 18% efficiency. Improvement in collection from the short wavelength region (400-500nm) may account for additional 1-2 mA/cm^2. Demonstration of laboratory cell efficiency above 18% facilitates the effort of attaining 15% flat plat modules.

Even though the results described above may favor one deposition scheme over another, or one device structure compared to another, we caution that more investigations into the variables affecting the different device structures and other deposition schemes are needed before a final conclusion is made. We expect, in

the near future, to expand on this theme. We also anticipate further improvement in device performance with further optimization of the window materials, and additional improvement in the absorber by the incorporation of sulfur.
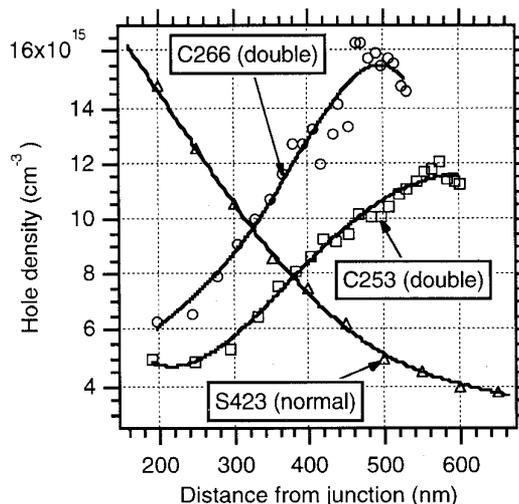
Figure 13. Carrier concentration as a function of distance from the junction

ACKNOWLEDGMENTS

REFERENCES

[1] J. Tuttle, M.A. Contreras, J.S. Ward, A.M. Gabor, K.R. Ramanathan, A.L. Tennant, L. Wang, J. Keane, and R. Noufi. These proceedings.

[2] John Scofield, S. Asher, D. S. Albin, J. Tuttle, M. Contreras, A. Tennant, D. Niles, R. Reedy, and R. Noufi. These proceedings.

[3] J. Kessler, K.O. Velthaus, M. Ruckh, R. Laichinger, and H.W. Schock. 6th International PVSEC. New Delhi, India, 1992, pp. 1005-1010.

[4] L. Stolt, J. Hedström, J. Kessler, M. Ruckh, K. Velthaus, and H. Schock. Appl. Phys. Lett. 62 (6), 8 February 1993, pp. 597-599.

[5] M. Contreras, J. Tuttle, D. Albin, A. Tennant, and R. Noufi. Proceedings of theTwenty-Third IEEE PVSC, 1993, pp. 486-490.

[6] A. Pawlikiewicz and S. Guha. *IEEE Transactions on Electronic Devices*, Vol. 37, No. 2, February 1990, pp. 403-409.

[7] M. Contreras, J. Tuttle, D. Du, Y. Qu, A. Swartzlander, A. Tennant, and R. Noufi. *Appl. Phys. Lett.* **63** (13), 27 September 1993, pp. 1824-1826.

[8] C. Jensen, D. Tarrant, J. Ermer and G. Pollock. *Twenty-Third IEEE PVSC*, 1993, pp. 577-580

[9] A. M. Gabor, J.R. Tuttle, D.S. Albin, R. Matson, A. Franz, D.W. Niles, M.A. Contreras, A.M. Hermann and, R. Noufi. Mat. Res. Soc. Symp. Proc., Vol. 343, 1994, pp. 143-148.

[10] A.M. Gabor, J.R. Tuttle, A. Schwaryzlander, A.L. Tennant, M.A. Contreras, and R. Noufi. These proceedings

[11] M. Contreras, A.M. Gabor, A. Tennant, S. Asher, J. Tuttle, and R. Noufi. *Progress in Photovoltaics*, Vol. 2, pp. 287-292, (John Wiley &Sons,1994).

[12] A. Gabor, J.R. Truttle, M. Contreras, D.S. Albin, A. Franz, D.W. Niles, and R. Noufi. *Proceedings from the 12th European Photovolaic Solar Energy Conference*

(H.S. Stephens and Assoc., UK), Amsterdam, The Netherlands, 11-15 April 1994, pp. 939-943.

[13] J. Tuttle, M. Contreras, A. Tennant, D. Albin, and R. Noufi. *Twenty-Third IEEE PVSC*, 1993, pp.415-421.

[14] A.M. Gabor, J.R. Tuttle, D. S. Albin, A. L. Tennant, M.A. Contreras, and R. Noufi. AIP Conference Proceedings 306, (AIP Press, New York), 1994, pp. 59-66.

[15] D. Schmid, M. Ruckh, F. Grunwald, and H.W. Schock. J. Appl. Phys. 73 (6), 15 March 1993, pp. 2902-2909.

[16] S. Wei and A. Zunger (internal communication). Data obtained from theoretical calculations based on local density formalism as implemented by Linear Augmented Plane Waves Method (S. Wei and A. Zunger, *Physical Review Letters*, Vol. 59, No. 1, 6 July 1987, p. 144).

[17] A. Dhingra and A. Rothwarf. *Twenty-Third IEEE PVSC*, 1993 pp. 475-480.

[18] P. Mauk, H. Tavakolian, and J. Sites. *IEEE Transactions On Electron Devices*, vol. 37, No. 2, February 1990, pp. 422.